Materials Today Advances 4 (2019) 100024

Contents lists available at ScienceDirect

Materials Today Advances

journal homepage: www.journals.elsevier.com/materials-today-advances/

Multiscale synchrotron scattering studies of the temperature-dependent changes in the structure and deformation response of a thermoplastic polyurethane elastomer

T. Sui [a], E. Salvati [b], H. Zhang [b], I.P. Dolbnya [c], A.M. Korsunsky [b, *]

[a] Department of Mechanical Engineering Sciences, University of Surrey, Guildford, Surrey, GU2 7XH, United Kingdom
[b] Department of Engineering Science, University of Oxford, Parks Road, Oxford, OX1 3PJ, United Kingdom
[c] Diamond Light Source, Harwell Campus, Didcot, OX11 0DE, United Kingdom

ARTICLE INFO

Article history:
Received 30 June 2019
Accepted 3 October 2019
Available online 27 November 2019

Keywords:
Thermoplastic polyurethane
Synchrotron X-ray scattering
Multi-scale characterization
Thermo-mechanical properties

ABSTRACT

The distinct molecular architecture and thermomechanical properties of polyurethane block copolymers make them suitable for applications ranging from textile fibers to temperature sensors. In the present study, differential scanning calorimetry (DSC) analysis and macroscopic stress relaxation measurements are used to identify the key internal processes occurring in the temperature ranges between −10 °C and 0 °C and between 60 °C and 70 °C. The underlying physical phenomena are elucidated by the small-angle X-ray scattering (SAXS) and wide-angle X-ray scattering (WAXS) study of synchrotron beams, allowing the exploration of the structure-property relationships as a function of temperature. *In situ* multiscale deformation analysis under uniaxial cyclic thermomechanical loading reveals a significant anomaly in the strain evolution at the nanoscale (assessed via SAXS) in the range between −10 °C and 0 °C owing to the 'melting' of the soft matrix. Furthermore, WAXS measurement of crystal strain within the hard regions reveals significant compressive residual strains arising from unloading at ~60 °C, which are associated with the dynamic shape memory effect in polyurethane at these temperatures.

1. Introduction

Thermoplastic polyurethanes (TPUs) are a versatile class of polymeric block copolymers that show an exceptional range of thermomechanical properties. Owing to their inherent adaptability, they are extensively used in applications such as textiles, sport shoes, biomedical implants, and temperature sensors. The typical morphological structure of TPUs consists of contiguous chains containing compliant soft segments (SSs) and much stiffer hard segments (HSs). The nanoscale arrangement of these chains leads to the formation of hard and soft regions with different packing densities, as illustrated in Fig. 1a, showing a high-resolution transmission electron microscopy (HRTEM) image of a polyurethane structure. The SS appears white, and the HS appears dark under the electron beam owing to the reaction with ruthenium tetraoxide on staining [1]. Three precursor components that made up this TPU are shown in Fig. 1b: 4,4′-dibenzyl diisocyanate (DBDI), polyethylene adipate (PEA), and ethylene glycol (EG). The self-organized structure of hard and soft nanoregions, together with the 'fuzzy' interfaces between them, can be thought of as a polymer nanocomposite [2–4].

The overall chemical, mechanical, physical, and thermal properties of TPUs originate in their nanoscale phase separation by the relative volume fraction of the HS and SS and intrinsic properties of each of the phases. The demand for high performance of polyurethanes led to increasing attention in investigating their structural features and functions, in particular, thermomechanical responses across multiple length scales. Existing challenges concern understanding the correlation between the conformation of polymeric chains, chain dynamics, nanoscale morphology, and macroscopic architecture, on the one hand, and the thermomechanical behavior and in-service performance sought in specific applications, e.g., stretchability and strain-induced crystallization, temperature-induced shape memory effects (SMEs), and so on, on the other hand.

Various experimental techniques allow characterizing the thermal transition and structural changes of TPUs, such as differential scanning calorimetry (DSC) [5, 6] and thermogravimetric

* Corresponding author.
E-mail address: alexander.korsunsky@eng.ox.ac.uk (A.M. Korsunsky).

https://doi.org/10.1016/j.mtadv.2019.100024

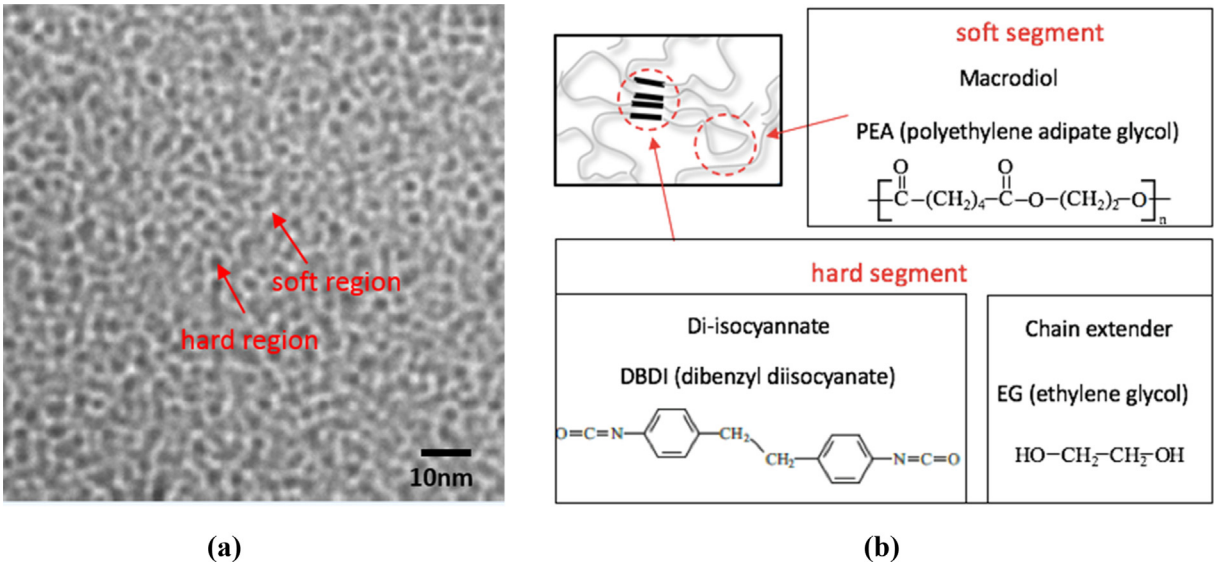

Fig. 1. **(a)** HRTEM image of a TPU (courtesy of Dr. Kayleen Campbell, University of Queensland) revealing the phase-separated morphology (schematic diagram of hard and soft regions). **(b)** The TPU system was made by mixing three precursor components: 4,4′-dibenzyl diisocyanate, polyethylene adipate, and ethylene glycol. HRTEM, high-resolution transmission electron microscopy; TPU, thermoplastic polyurethane.

analysis (TGA) [7]. Fourier-transform infrared spectroscopy (FTIR) has been used to help understand hydrogen bonding interactions in segmented polyurethanes [8–10]. Dynamic mechanical analysis (DMA) has been used to probe the micro-scale-/nanoscale phase separation. This is through changes in the thermal signature of the components and measuring the ability of the material to store or dissipate energy as a function of temperature. Extensive reports of research into the deformation behavior of TPUs are available [11–14]. However, these studies so far only focused on the macroscopic deformation and thermal response as a basis for hypothesizing about the structure and strain accommodation within TPUs at finer scales. Limited effort has been devoted to exploring the detailed response of each phase (hard and soft) at the microscale and at the nanoscale, as well as to understanding the relationship between the multiscale architecture and multiphase mechanical behavior. In fact, even when coupled stress-strain-temperature studies of semicrystalline polyurethane were conducted, they appear to have been limited only to the macroscopic scale [15].

The combination of different synchrotron X-ray techniques allows combined *in situ* analysis and elucidation of the fine connections between the evolution of material architecture and deformation at different dimensional scales. However, from the available studies on polyurethanes in the literature, it appears that X-ray techniques have only been used so far to characterize separately either the mechanical properties [16–18] or structural changes purely as a function of temperature [19–21]. A popular multimodal technique, the combined small-angle X-ray scattering (SAXS) and wide-angle X-ray scattering (WAXS) has been used to evaluate the structural evolution of polyurethane and other elastomers. However, it is often only used for *ex situ* sample state evaluation before and after simple monotonic deformation or heating/cooling history, rather than *in situ* observation throughout the thermomechanical loading history. Surprisingly, studies reporting *in situ* stress-strain-temperature evolution are very rare. The thermomechanical behavior of shape-memory polymers has been explored [22], but only to quantify the strain recovery rate or strain fixity rate by a specific thermomechanical loading history. It is evident, therefore, that there is a need to conduct investigations particularly with a view to understanding the underlying multiphysics phenomena, e.g., Mullins effect, SME, and other phenomena characteristic of this class of elastomers.

In our previous studies, we have investigated the mechanical behavior of TPUs subjected to *in situ* uniaxial monotonic [23] and *in situ* incremental cyclic loading conditions (Mullins effect) [24] at room temperature, using advanced synchrotron-based X-ray scattering techniques (SAXS/WAXS). The evolution of the multilevel structure of a polyurethane during tensile loading provided improved insight into length scale–dependent straining characterization and physical mechanisms responsible for observing the Mullins effect.

The relationship between the structure and thermomechanical properties of TPUs under repeated cyclic loading is investigated through systematic experimental synchrotron X-ray techniques. In particular, the present study examines the relationship between DSC and stress relaxation measurements at the macroscopic scale and elucidates how the structure and mechanical behavior are coupled at those temperature ranges at the nanoscale and atomic scale. This would provide the fundamental basis for the development of new high-performance polymer systems.

2. Materials and methods

2.1. Samples and laboratory experiments

The TPU formulation for the present study was produced at IMC (Iasi, Romania). The material was produced by mixing the following three precursor components: (1) a diisocyanate (DI) HS, namely, DBDI; (2) a macrodiol (MD) SS, namely, PEA MD (molecular weight = 2000 g/mol); and (3) a small molecule diol chain extender (CE), namely, EG (see Fig. 1). The molar proportions used in the synthesis were 4:1:3 (DI [DBDI]:MD [PEA]:CE [EG]), making ~40% mass fraction of the HS and an isocyanic index of I = 100, giving rise to a truly thermoplastic condition of the resulting polymer. First, DI and MD components were allowed to react by thorough mixing for 24 h at 100 °C in vacuum, to obtain a prepolymer consisting of MD terminated at each end with DI. The prepolymer was then thoroughly mixed for 24 h with the CE at 90 °C. The details of this particular synthesis route are given by Prisacariu et al. [25, 26]. The

material obtained in this way was placed into a closed mold and cured at 110 °C for 24 h to produce a sheet of ~1.0-mm thickness. After around 30 days of storage at room temperature, a strip sample denoted PU185H with the cross-sectional dimensions of 1.20×1.91 mm^2 and the total gauge length of 3 mm was cut from the sheet. DSC measurement was performed at the Laboratory for In situ Microscopy and Analysis (LIMA), Oxford, using TA Instruments DSC Q2000. The TPU sample was heated from zero heat flow of −90 °C at a heating rate of 20 °C/min to 250 °C [27], held isothermal for 3 min, followed by cooling to −60 °C at 10 °C/min (Fig. 2a and b). The stress relaxation test was carried out at Oxford using a compact tensile loading rig provided by Deben (Microtest; Deben Ltd, Suffolk, UK) with a >heating rate of 2 °C/min from 40 °C to 90 °C provided by the Peltier heating-cooling stage (see Fig. 2c).

2.2. In situ scattering thermo-mechanical properties

In situ multiscale observation of elastic and inelastic deformation at elevated temperatures of polyurethane was performed on B16 beamline at Diamond Light Source (DLS, UK). This was performed via the Deben heating-cooling stage with the Deben tensile loading rig and multimodal X-ray techniques (2D transmission SAXS and WAXS). The X-ray flux was maximized by the appropriate choice of a multilayer monochromator. A beam energy of 16.5 keV was used and collimated to 0.2 mm × 0.2 mm spot size. To observe the multiscale structural changes and thermomechanical response, the Deben Peltier heating-cooling stage was used at the following temperatures: 10 °C, 0 °C, 30 °C, 60 °C, 90 °C, and 120 °C (see Fig. 3). For each temperature, *in situ* loading-unloading was applied to the specimen using a Deben tensile loading rig with a 200-N calibrated load cell, with grips specially designed for this purpose, as shown in Fig. 3. The loading was applied in the following sequence: 0.05 N, 0.5 N, 1 N, 1.5 N, 2 N, 2.5 N, 2 N, 1.5 N, 1 N, 0.5 N, and 0.05 N. The load and crosshead displacement were recorded by the Deben Microtest package and were further transformed to obtain sample stress, extension, and strain. The Peltier heating-cooling stage was constrained such that the initial sample size could not be small; thus, the total displacement/strain is limited by the travel limit of the Deben rig. Therefore the structural-mechanical-thermal response at small strains is the primary focus in this study. Radiography images were acquired using a scientific CMOS camera (Photonic Science Ltd., UK), also known as the 'X-ray Eye,' making sure the beam spot was on the samples and the beam traveled from the side of the sample. At each loading increment, the ImageStar 9000 2D WAXS detector (Photonic Science Ltd., UK) was placed in the beam path, and diffraction patterns were acquired at the detector-to-sample distance of 178.8 mm. The precise distance was determined by obtaining patterns from NIST SRM 640d silicon powder and from NIST SRM 660a lanthanum hexaboride powder (LaB6). Translating the WAXS detector out of the beam path allowed exposing the Pilatus 300 K SAXS detector (Dectris, Baden, Switzerland) for transmission-mode SAXS pattern acquisition. The sample-to-detector distance was found to be 4545 mm by using the pattern from dry chicken collagen for calibration [28, 29]. The effect of viscoelasticity is not considered in this study as both SAXS and WAXS data acquisition took a few seconds and the overall data acquisition per strain point was less than a minute, taking into account the detectors' translation time.

2.3. Data interpretation

First, the data exported from Microtest software from Deben were used to calculate the macroscale strain of each sample, with individual dimensions taken into account. Then, the SAXS and WAXS patterns were postprocessed separately to obtain strains at different length scales.

Two-dimensional SAXS patterns were subjected to azimuthal integration over an angular range between −20° and 20° around the loading direction (0°) provided the 1D intensity function $I_{SAXS}(q)$, where q is the scattering vector. Peak center position q^* was determined by fitting the $I_{SAXS}(q)$ curve with Gaussian function, allowing the conversion of q^* to real-space structural dimension (d) using $d = 2\pi/q^*$. The discrete Bragg scattering peak position q^* was found to reflect the 'fuzzy interface' between hard and soft regions, where a quasi-periodic fluctuation in electron density within these materials could be assigned to the inter-domain spacing of the HS and SS domains. Therefore, the Bragg equation was used to estimate the characteristic morphological periodicity from the scattering vector corresponding to the SAXS peak position, which is related to the scattering angle and the wavelength of the X-rays. In another word, a 'long period' d can be calculated simply from $d = 2\pi/q^*$, representing a dominant repeat distance of the two-phase structure causing the scattering. Therefore, the change in q^* (and d) during repeated mechanical loading, compared with the reference value, could be used to make inferences regarding the structural evolution and the nanoscale strain ($\varepsilon_{SAXS} = \frac{d-d_0}{d_0}$, where d_0 was from the strain-free state).

The integration over a similar azimuthal angular range (± 20°) of 2D WAXS patterns around the loading direction was used to obtain 1D intensity profiles. The total intensity (I_{WAXS}) consisted of the sum

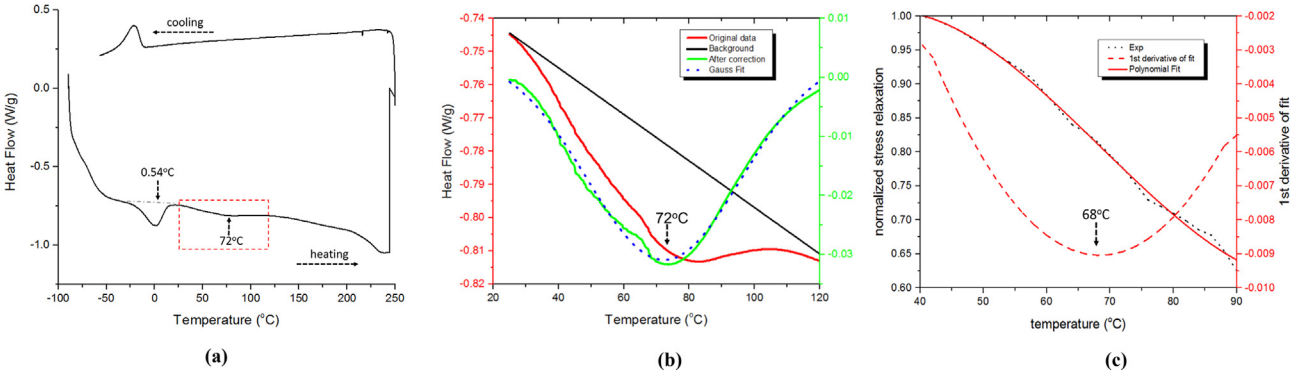

Fig. 2. Macroscopic thermomechanical test of TPU samples. **(a)** DSC plot of the TPU sample. The sample is heated up from −90 °C to 250 °C at a heating rate of 20 °C/min, held isothermal for 3 min, followed by cooling to −60 °C at 10 °C/min. The endothermic peak appears at 0 °C. **(b)** Zoomed-in version of the broad endothermal peak around 70 °C showing clear correlation with the temperature dependence of the stress relaxation derivative. The peak profile (green line) was corrected by subtracting the original data (red line) by the background (black line). **(c)** Stress relaxation test of the TPU sample. The stress is recorded at a constant distance (strain) while the sample was heated in the temperature range of 40 °C and 90 °C. TPU, thermoplastic polyurethane; DSC, differential scanning calorimetry.

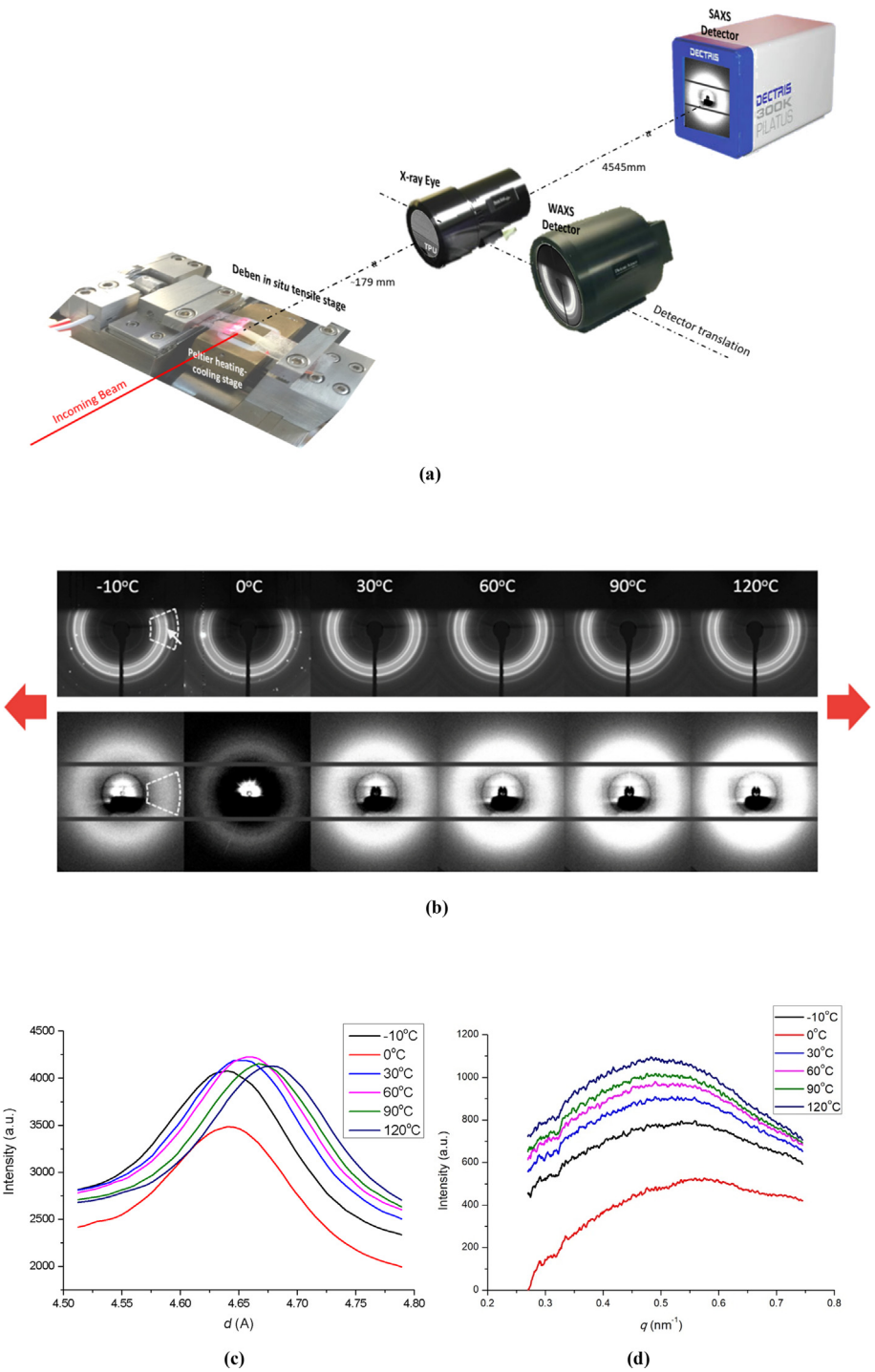

Fig. 3. ***In situ*** **thermomechanical characterization by SAXS and WAXS techniques. (a)** Schematic diagram of the multipurpose experimental beamline setup using the Deben Peltier heating-cooling stage combined with the loading rig. **(b)** Selected WAXS (fist row) patterns and SAXS patterns (second row) at maximum load (2.5 N) at the following temperatures: 10 °C, 0 °C, 30 °C, 60 °C, 90 °C, and 120 °C (loading direction indicated by solid red arrows). **(c)** One-dimensional WAXS profiles of the most prominent peak (indicated by white arrow in (b)) used for strain calculation. **(d)** One-dimensional SAXS profiles of the most prominent peak (indicated by white arrow in (b)) used for strain calculation. SAXS, small-angle X-ray scattering; WAXS, wide-angle X-ray scattering.

of crystalline diffraction (I_c) and amorphous scattering (I_a) components. The crystalline peak of the I_c curve could be clearly identified and analyzed by fitting the I_c curve with Gaussian peak function and determining the center positions after subtraction of the amorphous scattering component I_a and background. The atomic lattice strain (ε_{WAXS}) was then derived from the interplanar *d*-spacing changes, observed as the shift of the peak center position.

3. Results

The results of the DSC measurement shown in Fig. 2a reveal the following. Multiple DSC measurements were performed to verify reproducibility. Because the results were reproducible within measurement uncertainties, we present a single curve. The glass transition in this polymer is associated with a steep temperature

dependence of the heat flow seen around −63 °C. An endothermal peak was observed around 0 °C during heating and cooling. In the literature, this peak is reported to be associated with the melting and recrystallization process [3]. However, as will be clear from the results of material characterization reported in the following section, TPU is semicrystalline at all temperatures higher than the glass transition temperature. This apparent contradiction led us to conclude that the 'melting' of the material reported in the literature should be appropriately qualified as the crystalline-to-amorphous transition that occurs only in the soft regions (SRs) of the material. In contrast, the hard regions (HRs) remain crystalline in the entire temperature range between T_g and complete melting of the polymer.

In addition, a broad shallow endothermal peak is found in the DSC curve between ~60 °C and 90 °C. To make the peak more visible, Fig. 2b provides a zoomed-in view and helps identify the peak against a sloping background so that the peak center position around 70 °C becomes evident. The appearance of this peak must be associated with other conformational changes that occur at these temperatures. To reveal further connection between structural changes and mechanical behavior, macroscopic stress relaxation testing was carried out between 60 °C and 90 °C. In Fig. 2c, the experimental curve for stress relaxation as a function of temperature (shown in black dash), is accompanied by cubic polynomial fit (continuous red curve) and its derivative (red long dash). The clear conclusion is drawn that the fastest stress relaxation occurs at ~68 °C, indicating the tight link between the thermally driven structural changes and the mechanical response.

To elucidate the structure-thermomechanical relationship at finer scales of those particular temperature ranges (−10 °C to 0 °C and 60 °C–90 °C), *in situ* thermomechanical experimental investigation was conducted combined with imaging, SAXS and WAXS. The schematic diagram of the multipurpose beamline setup developed by the present researchers and used in a range of experimental *in situ* synchrotron studies is illustrated in Fig. 3a. The Deben Peltier heating-cooling stage combined with the Deben loading rig was used to study the thermomechanical response subjected to a sequence of uniaxial incremental tensile loading and unloading tests at different temperatures. The chosen load values were 0.05 N, 0.5 N, 1 N, 1.5 N, 2 N, 2.5 N, 2 N, 1.5 N, 1 N, 0.5 N, and 0.05 N, while the chosen temperatures were −10 °C, 0 °C, 30 °C, 60 °C, 90 °C, and 120 °C. An illustration of 2D SAXS and WAXS patterns at maximum load (2.5 N) at different temperatures is shown in Fig. 3b.

The evolution of the SAXS patterns with temperature is presented in Fig. 3b. Upon cooling, SAXS intensity is seen to become extremely low at 0 °C and remain weak at −10 °C. As demonstrated in a previous study [23], small-angle scattering in TPU is sensitive to the nature and volume fraction of the 'fuzzy interfaces' between the hard and soft regions, and SAXS intensity is proportional to the density contrast between the SRs and HRs in the material. Reduced SAXS intensity, as illustrated in Fig. 3b, is consistent with a decrease in the density differences. This can be explained by the reduction in the density gradients within the soft regions of the material or by a decrease in the amount of crystalline domains within the material. One-dimensional SAXS profiles of the most prominent peak are shown in Fig. 3d, and the strain values were found from peak center positions. This discrete Bragg scattering peak appears at a position of ~0.2–0.5 nm^{-1} of q range, which is consistent with works reported in the past [16,23,24].

The evolution of the WAXS patterns with temperature is presented in Fig. 3b. Isolated bright spots are observed in the patterns at −10 °C, which become more numerous at 0 °C, indicating the presence of large (micron-scale) crystallites. It is a long established and generally reported observation that the intensity of WAXS peaks from crystalline phases grows sharply with temperature as melting is approached. This is likely to be associated with the increase in the thermal motion amplitude of the scattering lattice planes [30]. The continuous Debye-Scherrer rings originate from nanocrystalline HRs that appear to remain substantively unchanged throughout the temperature range, with the exception of small changes in the lattice spacing associated with thermal and deformation phenomena. One-dimensional WAXS profiles of the most prominent peak is shown in Fig. 3c, and the accurate strain values were found from the peak center positions. Further discussion of the details of the observations made during *in situ* synchrotron scattering experiments and their interpretation are given in the following section.

The evolution of macroscopic strain over the cyclic loading history at incremental temperature conditions measured by the Deben rig is presented in Fig. 4. Fig. 4a plots stress vs. strain at different temperatures, revealing the energy dissipation between each loading-unloading hysteresis loop and also the residual strain of TPU after unloading at each temperature. No big difference in the gap has been observed as the temperature increases, indicating an almost constant dissipated energy. The residual strain after each load cycle varies with temperature, but the trend is found not to be monotonic. In general, tensile residual strain is observed at the macroscopic scale after each cycle, whereby a slight compressive residual strain occurs only at 60 °C after unloading. The original

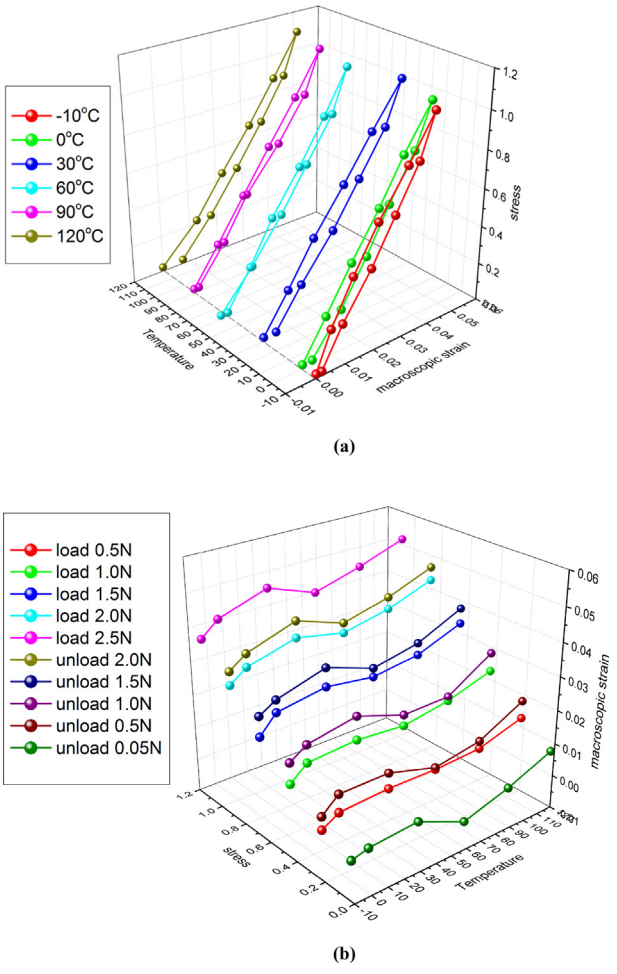

Fig. 4. The evolution of macroscopic strain. **(a)** Macroscopic strain evolution during one cycle of loading and unloading at different temperatures. **(b)** Macroscopic strain variation at different temperatures at each loading and unloading state.

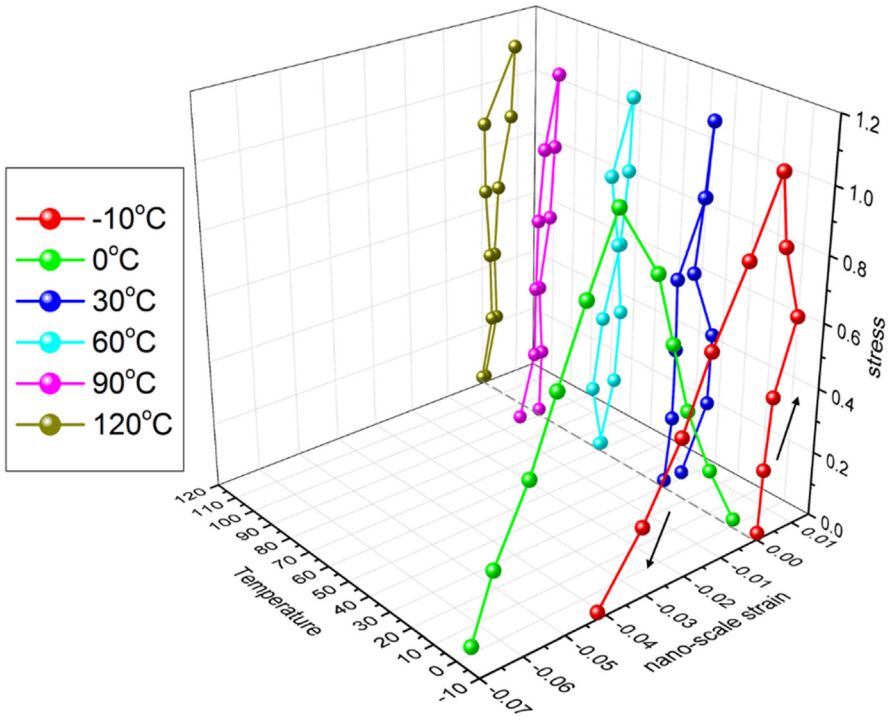

(a)

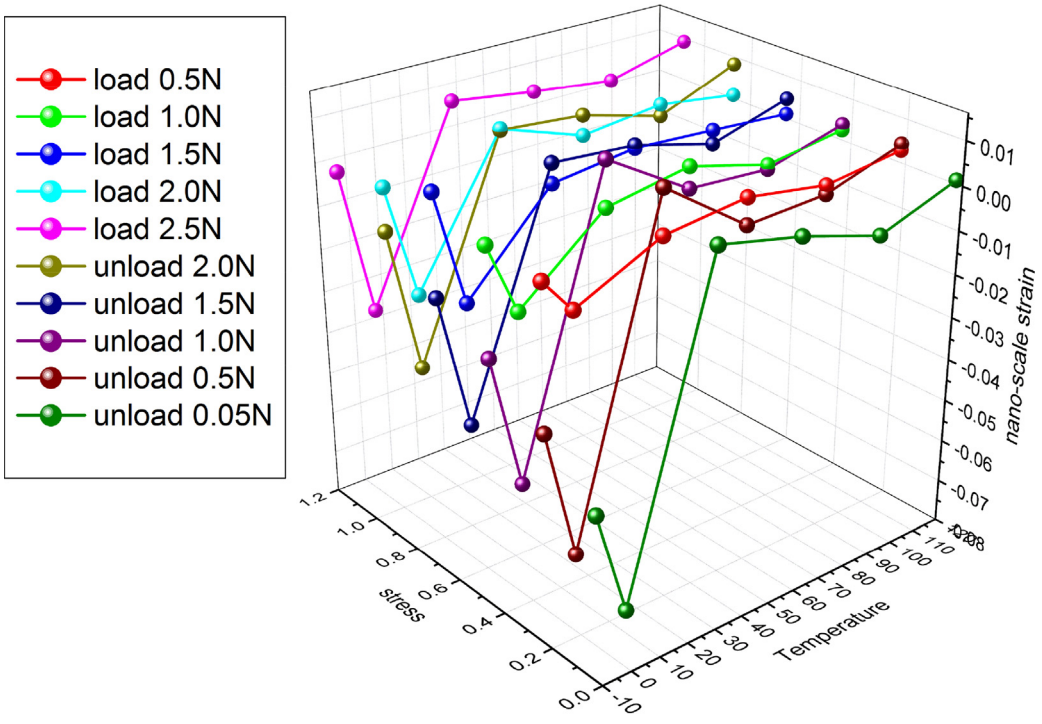

(b)

Fig. 5. Nanoscale strain deduced from SAXS pattern analysis. **(a)** Nanoscale strain evolution during a cycle of loading and unloading at different temperatures. **(b)** Nanoscale strain variation with temperature. SAXS, small-angle X-ray scattering.

data are replotted in Fig. 4b to reveal temperature vs. strain and its variation at different loading and unloading states. A valley consistently appears at 60 °C at each stress state and becomes more and more pronounced as the load increases.

The evolution of strain of the fuzzy interface between the SR and HR at the nanoscale level is calculated from SAXS patterns and is shown in Fig. 5. Fig. 5a displays the evolution of stress vs. strain at all the examined temperatures. Significant change of the strain can be observed during the load cycles at −10 °C and 0 °C, compared with those at other temperatures. In particular, the modulus (the slope of the curve) at 0 °C is even observed to be negative on loading (see the arrow direction in Fig. 5a). The diffraction spots appeared in Fig. 5b at −10 °C and 0 °C affect data interpretation, while the significant electron density changes at nanometer domains at 0 °C with the entire intensity of SAXS patterns reduced. Some positive residual strain occurs at 30 °C (~0.5%), whereas some negative residual strain with equal magnitude but opposite sign occurs at 90 °C after unloading. Fig. 5b then demonstrates the evolution of nanoscale strain with respect to the temperature at different loading and unloading stages. Strongly nonlinear evolution behavior can be seen particularly at −10 °C and 0 °C. However, no further trend can be clearly identified at temperatures higher than 0 °C.

Fig. 6 presents the variation of the atomic-scale strain from the crystalline regions or HRs within the material with temperature, as calculated from the WAXS patterns. The stress-strain curve during each load cycle is shown in Fig. 6a with two evident features. First, the strain is significantly lower than the strains at the nanoscale and macroscopic scales at all the tested temperatures as the strongly cross-linked HRs could be up to 100 times harder than the soft regions. Second, a positive residual strain accumulates at each unloading stage as the temperature increases until 30 °C, where the maximum positive residual strain reaches approximately 0.03%. However, a reverse trend is observed around 60 °C, at which the residual strain recovers and starts to accumulate in the opposite direction. The maximum negative residual strain is reached after unloading at 60 °C, with the value approximately −0.04%. Such a negative residual strain, however, is found to recover and accumulate in the positive direction again as the temperature increases further higher than 90 °C. Fig. 6b illustrates different atomic strain levels with increasing temperature, and an apparent valley can be observed at 60 °C at each stress state. This trend is consistent with that observed macroscopically (Fig. 4b), but the feature of the valley revealed by WAXS is more pronounced in the strain vs temperature plot.

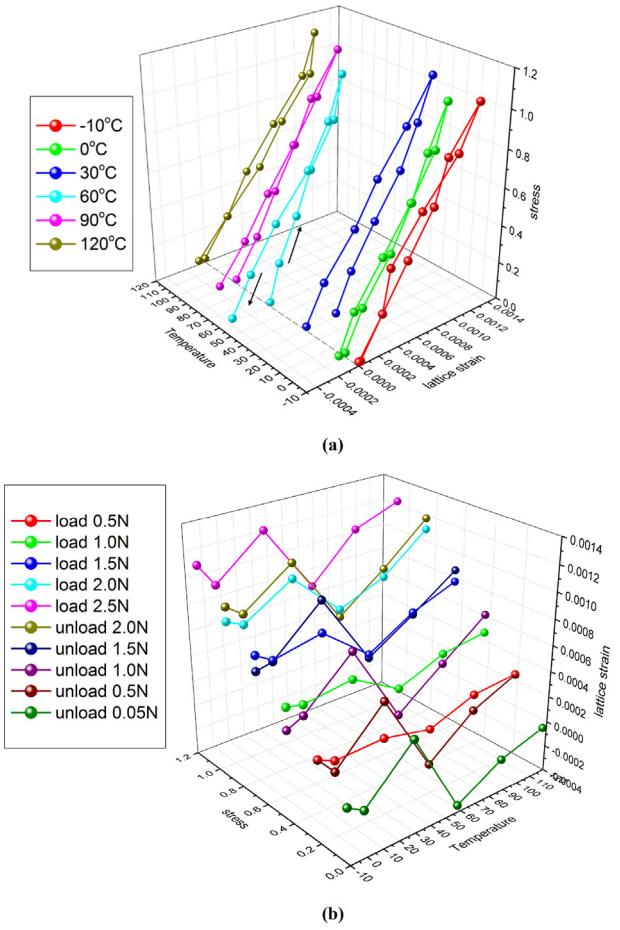

Fig. 6. Lattice-scale strain derived from the WAXS pattern analysis. (a) Atomic-scale strain evolution during a cycle of loading and unloading at different temperatures. **(b)** Atomic-scale strain variation with temperature. WAXS, wide-angle X-ray scattering.

4. Discussion

SAXS and WAXS observations allow explaining the different physical changes that occur in the temperature ranges of −10 °C to 0 °C and 60 °C–90 °C, in which interesting features were captured by DSC measurement and macroscopic stress relaxation tests. On the basis of these considerations, a schematic TPU model with the HR and SR is proposed in Fig. 7, which helps explain the full complement of data pertaining to the temperature-dependent evolution of the structure and deformation behavior.

At around −10 °C, some SRs become more ordered (highlighted in dark gray color in Fig. 7a) that contain HRs within them and preserve the orientation within the SR matrix over micron lengths. It is interesting to note that a degree of coherence appears between these SR crystallites and nanoscale HRs. Evidence comes from the lattice parameter correlation between individual reflections (soft microcrystals) and continuous Debye-Scherrer rings (hard nanocrystals) in the two leftmost WAXS patterns in Fig. 3b. Upon heating through 0 °C, these soft microcrystals melt, as shown in Fig. 7b, causing the appearance of the endothermal peak. The SR matrix becomes amorphous, leading to the increase in the SAXS intensity, which is also evident from Fig. 3b.

Another broad endothermal peak appeared in the DSC graph. The fast stress recovery that happened in the stress relaxation test at temperatures around 60 °C is ascribed to the dynamic SME in such a family of polyurethane. SME can appear within the SRs around this temperature [22, 31], which results in the mechanical interaction between the HR s and SRs. This also results in the negative nature of residual strain macroscopically as upon load removal, the polymer samples assume the length that is shorter than the original value. The origins of SME in polymers vary, and diverse mechanisms have been hypothesized [32]. In the case of polyurethane, most researchers agree that HRs act to store the elastic strain energy during deformation that is released when the surrounding amorphous matrix undergoes softening at temperature higher than the recovery temperature T_R, accommodating the required macroscopic strain. In our experiments, this hypothesis is confirmed via the evidence of significant strain recovery in the HRs, revealed by WAXS measurement. While structurally, the HRs remain unchanged, the broad endothermal peak at ~60 °C is clearly associated with enhanced mobility in the SR, as well as in the crucially important 'fuzzy interface' transition region [23].

Fig. 7c explains the mechanism of the reverse accumulation trend and occurrence of significant compressive residual strain around 60 °C at the atomic scale by WAXS and the macroscopic

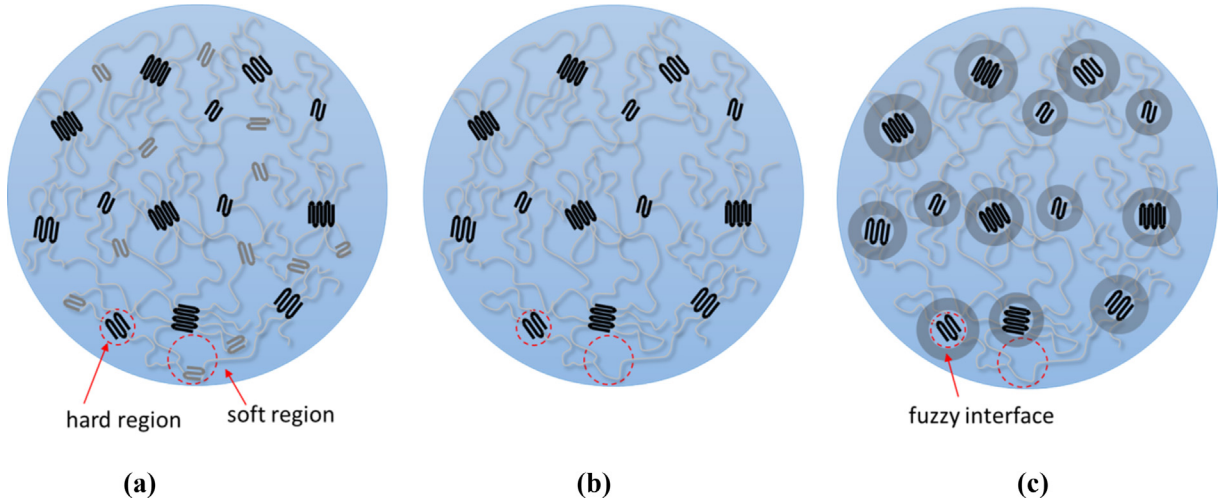

Fig. 7. Illustration of the structural evolution of hard and soft regions in a TPU representative volume: (a) at about −10 °C; (b) at about 0 °C, and (c) at about 60 °C, when the transition regions ('fuzzy interface') between HRs and the surrounding SRs acquire enhanced mobility and redistribute under loading, leading to temporary stiffening effect and strain recovery. TPU, thermoplastic polyurethane.

scale. The SRs with enhanced mobility around 60 °C will expand and redistribute around the HRs subjected to load. Some SRs may even aggregate at the boundary of HRs and lead to temporary hardening or stiffening effect for the HRs, resulting in the observed resistance to load or valley of the strain values appearing at this temperature from both atomic and macroscopic scales. The redistribution of the regions also modifies the mismatch between the HR and SR that generates the compressive residual strain in the HRs and affects the overall macroscopic residual strain state.

In addition, the conformational mobility of DBDI causes a wide range of characteristic properties, which are associated with the possibility of pronounced phase separation of inclusion-matrix morphology and with a high tendency to crystallization and self-association by hydrogen bonding. This is not available with the conventional DIs (e.g. 4,4′-diphenylmethane diisocyanate [MDI]) in traditional melt-cast polyurethanes. DBDI contains two methylene groups between the aromatic rings. The possibility of rotation around the central −C−C− bond allows more compact packing and crystallization between the DBDI HS blocks, thus producing substantial changes in properties. In contrast, MDI is intrinsically kinked in shape, reducing conformational mobility and thereby hindering close packing and achievement of hydrogen bonding. Tensile strength and residual elongation values were also found to be significantly higher for the DBDI-based PUs than those derived from MDI. This is because of a higher flow stress in the presence of DBDI, as can be associated with increased hydrogen bonding in DBDI-based polymers [2].

5. Conclusions

In summary, in this work, we explored the evolution of the hierarchical architecture of a polyurethane at the macroscale, nanoscale, and crystal lattice scales during cyclic thermomechanical processing by combined SAXS/WAXS techniques. The work gives *in situ* observational basis for improved insight into the structure-property relations for structural polymers such as TPUs. From this series of experiments, we identified the influence of temperature on the mobility of molecular chains that affects the macroscopic deformation response through changes in the conformation around HRs surrounded by the SR matrix. Findings include melting and recrystallization in the nanometer domains at low temperature, e.g., between −10 °C and 0 °C, which has been detected by DSC and confirmed by finer scale methods of SAXS and WAXS. The phenomenon, however, disappears at higher temperatures. The transition observed at temperatures higher than room temperature (around 60 °C) both in DSC and macroscopic stress relaxation tests was elucidated by X-ray scattering analysis. The increased mobility of soft regions at this temperature generates significant compressive residual strain of the HRs after unloading, which can be ascribed to the conformational mobility of DBDI. The findings open the way toward improved design and extended functionality for TPUs for future applications.

Author contributions

T.S. and A.M.K. formulated and planned the investigation. T.S., H.Z., E.S., and I.P.D. carried out *in situ* scattering experiments. T.S. carried out data analysis and wrote the manuscript with A.M.K. All authors contributed to editing the submission.

Data availability statement

The raw data required to reproduce these findings as well as processed data required to reproduce these findings are available from the authors on request.

Conflict of interest

The authors declare that they have no known competing financial interests or personal relationships that could have appeared to influence the work reported in this paper.

Acknowledgments

The authors wish to thank Dr Marzena Tkaczyk and Dr Kalin Dragnevski for their support in carrying out DSC measurements and Prof Cristina Prisacariu for material synthesis. The authors acknowledge the support of EPSRC RCUK via grants EP/I020691/1 and EP/P005381/1 and Diamond Light Source for the provision of access to beamline B16 under allocation MT12472-1. This article is dedicated to the memory of Cristina Prisacariu, who devoted her scientific life to the study of thermoplastic polyurethanes.

References

[1] S. Anandhan, H.S. Lee, Influence of organically modified clay mineral on domain structure and properties of segmented thermoplastic polyurethane elastomer, J. Elastomers Plastics 46 (2014).
[2] C. Prisacariu, Polyurethane Elastomers from Morphology to Mechanical Aspects, Springer, 2011, ISBN 978-3-7091-0514-6.
[3] C.B. Wang, S.L. Cooper, Morphology and properties of segmented polyether polyurethaneureas, Macromolecules 16 (1983) 775–786.
[4] B.X. Fu, B.S. Hsiao, S. Pagola, P. Stephens, H. White, M. Rafailovich, et al., Structural development during deformation of polyurethane containing polyhedral oligomeric silsesquioxanes (POSS) molecules, Polymer 42 (2011) 599–611.
[5] D. Nichetti, N. Grizzuti, Determination of the phase transition behavior of thermoplastic polyurethanes from coupled rheology/DSC measurements, Polym. Eng. Sci. 44 (2004) 1514–1521.
[6] S. Yamasaki, D. Nishiguchi, K. Kojio, M. Furukawa, Effects of aggregation structure on rheological properties of thermoplastic polyurethanes, Polymer 48 (2007) 4793–4803.
[7] M. Strankowski, D. Wlodarcyk, L. Piszczyk, J. Strankowska, Thermal and mechanical properties of microporous polyurethanes modified with reduced graphene oxide, Int. J. Polym. Sci. (2016) 2016.
[8] P.J. Yoon, C.D. Han, Effect of thermal history on the rheological behavior of thermoplastic polyurethanes, Macromolecules 33 (2000) 2171–2183.
[9] Y.X. Wang, M. Gupta, D.A. Schiraldi, Oxygen permeability in thermoplastic polyurethanes, J. Polym. Sci. Part B: Polym. Phys. 50 (2012) 681–693.
[10] I. Yilgör, E. Yilgör, G.L. Wilkes, Critical parameters in designing segmented polyurethanes and their effect on morphology and properties: a comprehensive review, Polymer 58 (2015) A1–A36.
[11] A. Saiani, C. Rochas, G. Eeckhart, W.A. Daunch, J.W. Leenslag, J.S. Higgins, Origin of multiple melting endotherms in a high hard block content polyurethane. 2. Structural investigation, Macromolecules 37 (2014) 1411–1421.
[12] A. Eceiza, M. Larranaga, K. de la Caba, G. Kortaberria, C. Marieta, M.A. Corcuera, et al., Structure-property relationships of thermoplastic polyurethaneelastomers based on polycarbonate diols, J. Appl. Polym. Sci. 108 (2008) 3092–3103.
[13] A. Mishra, P. Maiti, Morphology of polyurethanes at various length scale: the influence of chain structure, J. Appl. Polym. Sci. 120 (2011) 3546–3555.
[14] C.P. Buckley, C. Prisacariu, C. Martin, Elasticity and inelasticity of thermoplastic polyurethane elastomers: sensitivity to chemical and physical structure, Polymer 51 (2015) 3213–3224.
[15] N. Mirtschin, T. Pretsch, Designing temperature-memory effects in semicrystalline polyurethane, RSC Adv. 5 (2015) 46307–46315.
[16] K. Kojio, K. Matsuo, S. Motokucho, K. Yoshinaga, Y. Shimodaira, K. Kimura, Simultaneous small-angle X-ray scattering/wide-angle X-ray diffraction study of the microdomain structure of polyurethane elastomers during mechanical deformation, Polym. J. 43 (2011) 692–699.
[17] T. Kamal, C.Y. Park, M.C. Choi, Y.W. Chang, An in-situ simultaneous SAXS and WAXS survey of PEBAX (R) nanocomposites reinforced with organoclay and POSS during uniaxial deformation, Polymer 53 (2012) 3360–3367.
[18] H. Zhang, A.K. Scholz, Y. Merckel, M. Breu, D. Berghezan, E.J. Kramer, et al., Strain induced nanocavitation and crystallization in natural rubber probed by real time small and wide angle X-ray scattering, J. Polym. Sci. Polym. Phys. Ed. 51 (2013) 1125–1138.
[19] S. D'hollander, C.J. Gommes, R. Mens, P. Adriaensens, B. Goderis, F. Du Prez, Modeling the morphology and mechanical behavior of shape memory polyurethanes based on solid-state NMR and synchrotron SAXS/WAXD, J. Mater. Chem. 20 (2010) 3475–3486.
[20] A. Feula, X.G. Tang, I. Giannakopoulos, A.M. Chippindale, I.W. Hamley, F. Greco, et al., An adhesive elastomeric supramolecular polyurethane healable at body temperature, Chem. Sci. 7 (2016) 4291–4300.
[21] J. Silva, D. Meltzer, J. Liu, M. Cox, J. Maia, The influence of thermo-mechanical history on structure development of elastomeric and amorphous glass thermoplastic polyurethanes, Polym. Eng. Sci. 54 (2013) 1383–1393.
[22] C. Liu, H. Qin, P.T. Mather, Review of progress in shape-memory polymers, J. Mater. Chem. 17 (2007) 1543–1558.
[23] T. Sui, N. Baimpas, I.P. Dolbnya, C. Prisacariu, A.M. Korsunsky, Multiple-length-scale deformation analysis in a thermoplastic polyurethane, Nat. Commun. 6 (2015).
[24] T. Sui, E. Salvati, S. Ying, G. Sun, I.P. Dolbnya, K. Dragnevski, et al., Strain softening of nano-scale fuzzy interfaces causes Mullins effect in thermoplastic polyurethane, Sci. Rep. 7 (2016) 916.
[25] C. Prisacariu, R.H. Olley, A.A. Caraculacu, D.C. Bassett, C. Martin, The effect of hard segment ordering in copolyurethane elastomers obtained by using simultaneously two types of diisocyanates, Polymer 44 (2003) 5407–5421.
[26] C. Prisacariu, C.P. Buckley, A.A. Caraculacu, Mechanical response of dibenzyl-based polyurethanes with diol chain extension, Polymer 46 (2005) 3884–3894.
[27] Scortanu E. Prisacariu, Structural Studies and the Correlation with the Stress–Strain Response in Polyurethanes, John Wiley & Sons, Ltd, 2006, pp. 1–24.
[28] M.J. Berger, J.H. Hubbell, S.M. Seltzer, J. Chang, J.S. Coursey, R. Sukumar, et al., XCOM: Photon Cross Section Database 1.2, 1999. http://physicsnistgov/xcom.
[29] J. Bolze, J. Kim, J.Y. Huang, S. Rah, H.S. Youn, B. Lee, et al., Current status of the synchrotron small-angle X-ray scattering station BL4C1 at the Pohang Accelerator Laboratory, Macromol. Res. 10 (2002) 2–12.
[30] P.K. Sullivan, J.J. Weeks, The intensity as a function of temperature of the low-angle X-ray diffraction maxima of the n-paraffins: hexatriacontane, tetratetracontane, and tetranonacontane, J. Res. Natl. Bur. Stand. - A. Phys. Chem. 74A (1970).
[31] J. Kunzelman, T. Chung, P.T. Mather, C. Weder, Shape memory polymers with built-in threshold temperature sensors, J. Mater. Chem. 18 (2008) 1082–1086.
[32] X. Wu, W.M. Huang, Y. Zhao, Z. Ding, C. Tang, J.L. Zhang, Mechanisms of the shape memory effect in polymeric materials, Polymer 5 (2013) 1169–1202.